# RSC Pharmaceutics



### **PAPER**

View Article Online
View Journal | View Issue



Cite this: RSC Pharm., 2025, 2, 124

# Herceptin-conjugated plasmonic gold nanocapsules for targeted NIR-II photothermal therapy†

Prem Singh, D Ankita Sarkar, Nivedita Mukherjee and Amit Jaiswal D\*

In recent years, researchers have extensively studied nanomaterials for plasmonic photothermal therapy (PPTT), with most of the research focused on those active in the near-infrared I (NIR I) window ( $\lambda$  = 650–950 nm). However, there is growing interest in developing nanomaterials that are active in the near-infrared II (NIR II) region ( $\lambda$  = 950–1300 nm) due to the better penetrability and higher tolerance limit of NIR II light by human skin. In this study, the potential of gold nanocapsules (Au Ncap) with a rattle-like structure, consisting of a solid gold bead core and a porous, thin, rod-shaped gold shell was investigated for PPTT. Specifically, the targeted *in vitro* photothermal activity of Herceptin-conjugated gold nanocapsules that are active in both the NIR I and II regions are explored towards the Her2 positive SK-BR-3 breast cancer cell line. The conjugation of SH-PEG and Herceptin molecules on the surface of gold nanocapsules was validated through a detailed X-ray photoemission spectroscopy (XPS) analysis. The Au Ncap exhibited high photothermal conversion efficiency of 38.6% and *in vitro* PPTT results showed its excellent cytotoxicity against the SK-BR-3 cell line leading to apoptotic cell death. These findings suggest that this nanostructure can serve as an efficient photothermal agent in the NIR II region showing excellent PPTT activity at a low laser power density of 0.5 W cm<sup>-2</sup>.

Received 27th August 2024, Accepted 15th November 2024

DOI: 10.1039/d4pm00244j

rsc.li/RSCPharma

### 1. Introduction

In recent years, plasmonic gold nanostructures have gained immense attention in the field of photothermal therapy (PTT), particularly for cancer treatment. PTT is a non-invasive method that generates heat and selectively kills cancer cells by using light-absorbing substances. Gold nanoparticles exhibit unique optical properties that make them an excellent candidate for PTT. he localized surface plasmon resonance (LSPR) phenomenon exhibited by gold nanomaterial enables them to absorb light and transform it into heat. This heat can be used to kill cancer cells while causing minimal damage to surrounding healthy tissue. Moreover, the ease of synthesis and functionalization of gold nanomaterials make them an attractive candidate for use in biomedical applications. As 15,17

The near-infrared (NIR) light is favoured for PTT due to its ability to penetrate deep into tissues without causing significant tissue damage. Within the NIR range, the NIR I window ( $\lambda$ 

School of Biosciences and Bioengineering, Indian Institute of Technology Mandi, Kamand, Mandi-175075, Himachal Pradesh, India. E-mail: j.amit@iitmandi.ac.in †Electronic supplementary information (ESI) available. See DOI: https://doi.org/ 10.1039/d4pm00244j = 650–950 nm) has been the focus of research for PTT in cancer treatment for several years.  $^{2,8,14}$  However, because NIR I light have a restricted penetration depth, it is difficult to target deeply placed tumors. The NIR II window ( $\lambda$  = 1000–1350 nm), on the other hand, has a higher penetration depth and lesser scattering, making it more ideal for deep-tissue imaging and therapy.  $^{13,18-24}$  As a result, there is an increasing interest in developing NIR II-active nanomaterials for PTT.

In the NIR I window, gold nanoparticles have been intensively studied as a photothermal agent for PTT. <sup>3,20,25,26</sup> However, their performance in the NIR II window is still under scrutiny. The synthesis of gold nanomaterials with plasmon resonance in the NIR II region is intriguing due to the low absorption cross-section of gold nanomaterials in this range. <sup>19,22,27,28</sup> Therefore, it is essential to make gold nanomaterials with plasmon resonance in the NIR II region for PTT in deep-tissue cancer treatment. <sup>21–23,29,30</sup>

To address this challenge, plasmonic gold nanocapsules (Au Ncaps) were used for photothermal therapy (PTT) in the NIR I and NIR II regions, allowing effective PTT at low laser power density. These Au Ncaps have a unique structure, with a solid gold core inside a thin, porous gold shell. The surface of the Au Ncaps was functionalized with Herceptin (HER) to target Her2-positive breast cancer cells, enhancing the

**RSC Pharmaceutics** Paper

localized killing of cancer cells. The biocompatibility of the Au Ncaps was evaluated, and the mechanism of photothermalinduced cell death was also investigated.

#### **Experimental details** 2.

### 2.1. Materials

Gold(III) chloride trihydrate (HAuCl<sub>4</sub>·3H<sub>2</sub>O), benzyldimethylhexadecylammonium chloride (BDAC), citric acid, sodium borohydride (NaBH<sub>4</sub>), L-ascorbic acid, penicillin-streptomycin (Pen-Strep), Antibiotic-Antimycotic (Anti-Anti), fetal bovine serum (FBS), 1-ethyl-3-(3-dimethylaminopropyl) carbodiimide (EDC), N-hydroxysuccinimide (NHS), 0.25% trypsin-ethylenediaminetetraacetic acid (EDTA), sodium pyruvate, and Cell Proliferation Assay Kit II (XTT) were procured from Sigma-Aldrich. CTAC was procured from TCI, while carboxy PEG thiol (MW 5k) was acquired from JenKem Technology. McCoy's 5A culture media was obtained from Cell Clone. Amicon Ultra Centrifugal Filter Units (3 kDa and 10 kDa) were supplied by Merck Millipore. All synthesis procedures and experiments were conducted using ultrapure water (resistivity 18.2 M $\Omega$  cm) and glassware pre-cleaned with aqua regia.

#### 2.2. Instrumentation

Transmission electron microscopy (TEM) images were captured using a TEM instrument (FP 5022/22-Tecnai G2 20 S-TWIN, FEI, USA). Scanning electron microscopy (SEM) images of the synthesized nanostructures were obtained using a Nova Nano SEM-450 (FEI). The extinction spectra of the nanoparticles were recorded using a UV-vis NIR spectrophotometer (UV-1800, Shimadzu, Japan). The XPS was performed using a Nexsa G2 Surface Analysis System (X-ray photoelectron spectroscopy, XPS, Thermo Scientific) equipped with a microfocused X-ray monochromatic Al Kα source, a hemispherical analyzer, and a 128-channel plate detector. The XPS spectra were deconvoluted using Avantage software. Inductively Coupled Plasma Mass Spectrometry (ICP-MS) analysis for cellular uptake of nanoparticles was conducted at Agilent Technologies, Manesar, Gurugram, India.

### 2.3. Synthesis and surface modification of the synthesized gold nanocapsules utilizing monoclonal antibody trastuzumab (Herceptin)

Gold nanocapsules were synthesized using a previously reported three-step seed-mediated approach previously established by our group. 19 Initially, a gold nanobead was prepared using thermally twinned seed onto which a rod shaped silver shell was grown. The silver shell was then replaced with gold through a Galvanic replacement reaction which resulted in the formation of thin porous hollow shell around solid gold bead. This resulted in the formation of gold nanocapsules. Following the galvanic replacement reaction, the gold nanocapsules were washed by centrifugation at 5000 rpm for 10 minutes and then resuspended in an equal volume of ultrapure water. After synthesis, a dichloromethane (DCM) phase

separation technique was employed to remove excess surfactant from the nanoparticle solution. The purified nanocapsules were separated from the organic phase by an aqueous layer, rinsed with ultrapure water, and stored for future use.

In order to functionalize the prepared Au nanocapsules, the -COOH terminal of bifunctional PEG (COOH-PEG5000-SH) was activated using a carbodiimide crosslinker, 1-ethyl-3-(3-dimethylaminopropyl) carbodiimide (EDS) N-hydroxysuccinimide (NHS), by mixing equal molar concentrations (330 µM each) of COOH-PEG-SH, EDC, and NHS. After 2 hours of incubation at 4 °C, the free EDC and NHS were removed from the solution using a 3 kDa Amicon membrane filter, and the activated COO- terminal PEG thiol molecules were kept for further processing. These activated PEG thiol molecules were then mixed with Herceptin at a physiological pH of 7.4 and stored at 4 °C for subsequent conjugation with SH-PEG molecules. After 6 hours of incubation, a 10 kDa Amicon membrane filter was used to remove the free PEG thiol from the solution. Finally, Herceptin-conjugated PEG was tethered to the Au Ncaps using the sulfhydryl group of these polymers (Scheme 1). Specifically, the centrifuged pellet of the DCM-washed gold nanocapsules was resuspended in the PEG-HER conjugate solution, centrifuged again at 5000 rpm for 10 minutes, and stored overnight at 4 °C. The following day, the solution was centrifuged once more and rinsed with ultrapure water to remove the unbound PEG-HER conjugate.

The non-conjugated Au Ncaps were made biocompatible by incubating them overnight at 4 °C with an 330 µM of m-PEG5000-SH. The unbound m-PEG5000-SH was then removed by washing the nanoparticles with nanopure water, and the purified nanoparticles were stored at 4 °C for subsequent in vitro experiments.

### 2.4. Evaluation of photothermal performance of Au Ncap

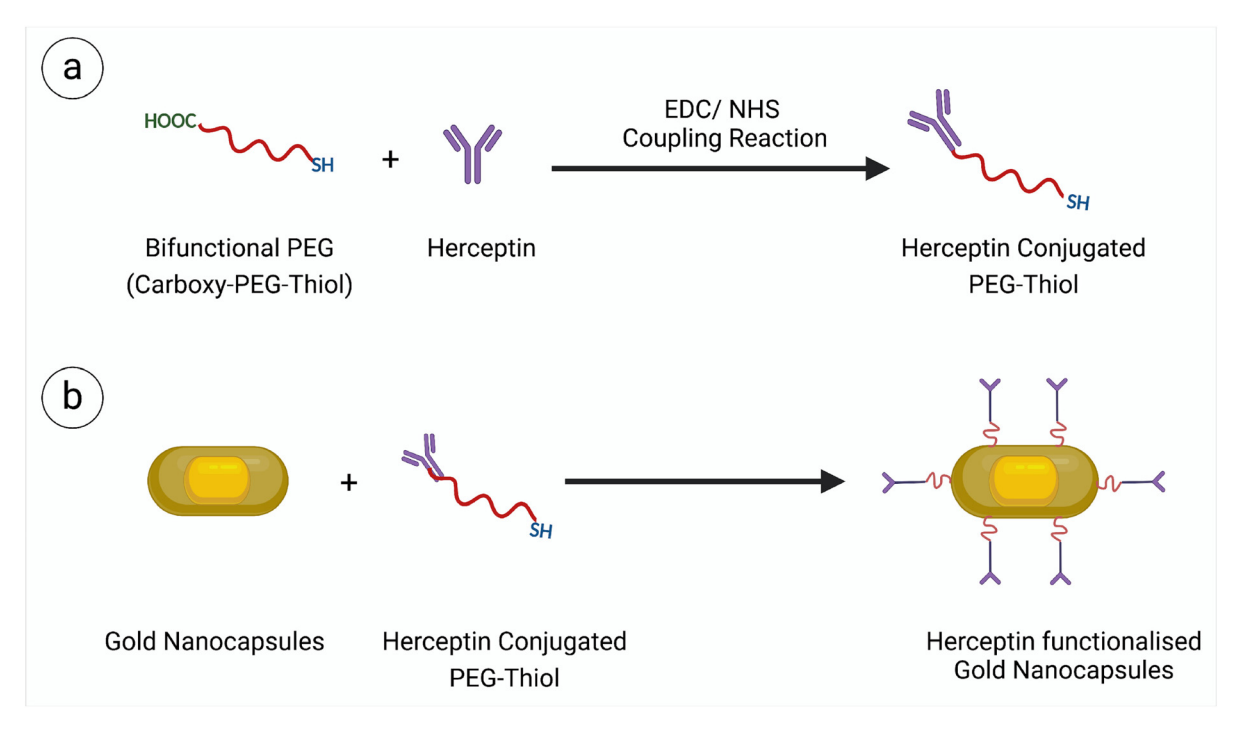
A 0.2 mL centrifuge tube containing 100 μL of Au Ncap - HER solution at varying concentrations was placed under a 1064 nm laser with different power densities. The temperature of the solution was then measured using a digital thermocouple thermometer (Make: RoHS, S. no. 201703014973). The thermal images of the gold nanocapsules following laser irradiation were captured using a thermal infrared camera (TESTO 875).

### 2.5. Cell culture

The Her2-overexpressed human breast cancer cell line SK-BR-3 was used as the cancer model, while HEK-293A cells were employed as the healthy control. SK-BR-3 cells were cultured in McCoy's medium supplemented with 10% v/v FBS and 1% v/v antibiotic in an incubator with 5% CO2 maintained at 37 °C. HEK-293A cells were cultured in Dulbecco's modified Eagle's medium (DMEM) supplemented with 10% v/v FBS and 1% v/v antibiotic (Pen-Strep).

### 2.6. Cell viability assay

HEK-293A and SK-BR-3 cells were seeded at a density of 10 000 cells per well in a 96-well culture plate to assess cellular bioPaper RSC Pharmaceutics



Scheme 1 Schematic demonstrating the synthesis of Herceptin conjugated gold nanocapsules.

compatibility. After 24 hours of incubation, the cells were treated with varying concentrations of Herceptin-conjugated gold nanocapsules (Au Ncap-HER) and incubated for an additional 24 hours in a  $\rm CO_2$  incubator. Following this incubation period, the nanoparticle containing media was removed from the cells by washing with PBS, XTT based cell viability was performed following the manufacturer's protocol. All experiments were conducted in triplicate, and the percentage of viable cells was calculated using the following equation:

$$\% \ cell \ viability = \frac{Absorbance \ of \ treated \ cells}{Absorbance \ of \ control \ cells} \times 100.$$

### 2.7. Evaluation of In vitro PPTT performance of Au Ncap

SK-BR-3 cells were cultured in a 96-well culture plate at a density of 10 000 cells per well for 24 hours after which it was treated with the Au Ncap-HER conjugate. After 6 h of incubation, the remaining nanoparticles-containing media were removed from the plates and the cells were rinsed with PBS, replaced with new media, and then exposed to a 1064 nm NIR laser at 0.5 W cm $^{-2}$  for 10 minutes. The cells were then placed in an incubator and kept there for 18 hours at 37 °C and 5%  $\rm CO_2$  atmosphere. The percentage of cell viability of the treated and control cells was then determined using an XTT-based cell viability test.

## 2.8. Evaluating the cell death mechanism through flow cytometry based annexin-V-FITC/PI assay and cell morphology analysis using SEM

SK-BR-3 cells were seeded at a density of  $0.5 \times 10^6$  cells per well in a 6-well plate for flow cytometric analysis and incu-

bated overnight. The following day, the media was removed, and the cells were treated with 100  $\mu g$  mL<sup>-1</sup> Au Ncap-HER in fresh media and incubated for 6 hours before being washed with PBS. Subsequently, the cells were exposed to NIR laser (1064 nm, 0.5 W cm<sup>-2</sup>, 10 min) and incubated for 12 hours. Non-irradiated cells served as the control for the experiment. After incubation, the treated cells were collected by centrifugation at 1000 rpm for 5 minutes following a PBS wash, stained with annexin V-FITC/PI according to the manufacturer's protocol. The stained cells were then acquired in a flow cytometer (BD LSRFortessa), with 10 000 events recorded per sample and analyzed using BD FACSDiva software.

To evaluate the cellular morphology of treated and untreated cells, SK-BR-3 cells were cultured on a glass coverslip at a density of  $0.5 \times 10^6$  cells per mL, followed by nanoparticle treatment and NIR laser irradiation. After 12 hours of laser treatment, the cells were rinsed with PBS, fixed with glutaral-dehyde for 2 hours, and then subjected to ethanol dehydration and drying. The cellular morphology of the fixed and dehydrated cells was then examined using SEM (Nova Nano SEM-450, FEI), with untreated SK-BR-3 cells serving as a control.

### Results and discussion

### 3.1. Synthesis of gold nanocapsules and its conjugation with monoclonal antibody trastuzumab (Herceptin)

Firstly, pentatwinned gold seeds with were prepared using CTAC as surface capping agents and in the presence of citric acid. The mechanism for obtaining twinned seeds involved **RSC Pharmaceutics** 

thermal treatment at 90 °C and the use of a citric acid. Subsequently, the nanosized gold seeds were utilized to synthesize gold nanobeads in the presence of BDAC as a surface capping agent. In the following step, these gold nanobeads served as a template for the growth of a silver metal shell, forming bimetallic nanorods with a silver coating on the surface of the gold nanobeads. Finally, a galvanic exchange reaction 18,26,31 was employed to remove the silver shell using gold salt, resulting in the formation of gold nanocapsules. 19 Fig. 1(a) represents the UV-Vis NIR extinction spectra of Au Ncap which clearly depicts that the Au Ncap have absorption both in the NIR I and NIR II regions. Fig. 1(b) represents the TEM image of the synthesized gold nanocapsules which clearly represents the capsular shape of the prepared particles consisting of a solid gold bead caged inside a thin porous hollow gold shell. Fig. S1† represents the SEM image of the gold nanocapsules, clearly depicting their surface topography, including the hollow and porous nature of the structures. From the SEM image, we calculated the mean size of the gold nanocapsules, which was found to be 110 nm  $\pm$  6 nm.

For *in vitro* targeted photothermal therapy applications, the surface of the Au Ncap was modified with Herceptin (Trastuzumab), which specifically binds to the Her2 receptors overexpressed on the surface of SK-BR-3 breast cancer cells. To accomplish this, the prepared Au Ncap was first washed using

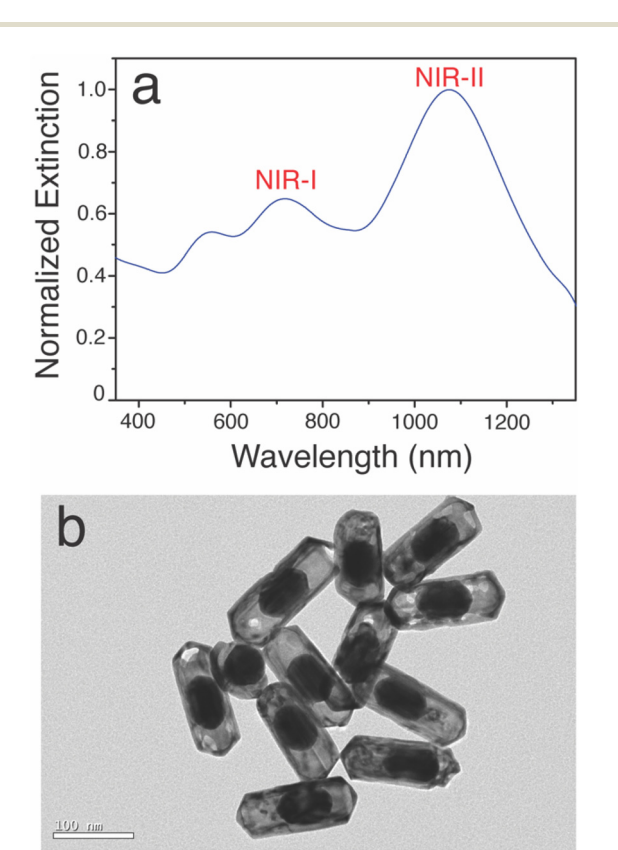


Fig. 1 (a) Extinction spectra of the synthesized gold nanocapsules and (b) TEM image of the gold nanocapsule. Scale bar corresponds to

a phase separation technique with DCM, rewashed, and resuspended in ultrapure water. The bifunctional SH-PEG5000-COOH was then activated in the presence of a carbodiimide 1-ethyl-3-(3-dimethylaminopropyl) crosslinker, namely carbodiimide (EDS) and N-hydroxy succinimide (NHS), to facilitate the conjugation of Herceptin to the -COOH terminal through an amide bond between Herceptin and the bifunctional PEG molecule. 32,33 Subsequently, the SH-PEG-Herceptin conjugate was tethered to the gold nanocapsules by utilizing its sulfhydryl terminal to form metal-sulfide bonds with the gold.34 UV-vis NIR spectroscopy, and XPS analysis were performed to validate the conjugation of the Au Neap with SH-PEG-Herceptin. A slight red shift in the localised surface plasmon resonance (LSPR) band of the Herceptin-conjugated gold nanocapsules was observed (Fig. 2a), which can be attributed to the change in the refractive index surrounding the Au Ncap, causing a red shift in the plasmonic band after Herceptin conjugation.

Further detailed XPS characterization was performed to confirm the presence of SH-PEG-Herceptin conjugate on the surface of the gold nanocapsules. The survey scan of Herceptin-conjugated Au Ncap (Au Ncap-HER) revealed additional peaks in the N 1s and S 2p regions (Fig. 2b & c). Additionally, an increase in the percentage of C 1s and O 1s regions was observed in Au Ncap-HER (Fig. 2c). Table S1† provides a summary of the area under the curve for the C 1s, O 1s, N 1s, and S 2p regions for both bare Au Ncap and Au Ncap-Her. After calculating the area percentages, we found a 20% increase in the intensity of the C 1s region and approximately a sixfold increase in the O 1s region, indicating the presence of the long-chain polymer PEG on the surface of the gold nanocapsules (Table S1†). High-resolution XPS spectra of the S 2p region demonstrated the formation of a bond between the metal and the sulfhydryl group. A splitting doublet in the S 2p region was identified at 162 eV, with the first split at 161.98 eV corresponding to the S 2p3/2 region and the second split at 162.8 eV corresponding to the S  $2p_{1/2}$  region (Fig. 2d). This confirmed that thiols were chemically bound to the gold metal via Au-S bonds.<sup>32</sup> Additionally, a peak at 161.38 eV was observed, representing free metal sulfides. In the N 1s region, the high-resolution XPS spectra also revealed the formation of amide bonds at 399.3 eV (Fig. 2e), indicating the presence of protein antibodies on the surface of the gold nanocapsules.<sup>32</sup> These findings clearly validated the successful conjugation of Herceptin molecules to the Au Ncap.

### 3.2. Evaluation of the photothermal property of the synthesized gold nanocapsules

Since these Au Ncaps exhibited high absorption in the NIR II region, a 1064 nm laser was employed to assess the photothermal heating capability of the Au Ncaps in an aqueous solution. To accomplish this, the temperature increase of the Au Ncap aqueous solution was measured upon irradiation with 1064 nm laser at various laser power densities ranging from 0.5 W cm<sup>-2</sup> to 3 W cm<sup>-2</sup>, with the Au Ncap concentration maintained at 50 µg mL<sup>-1</sup> (Fig. 3a). Following 6 minutes of Paper

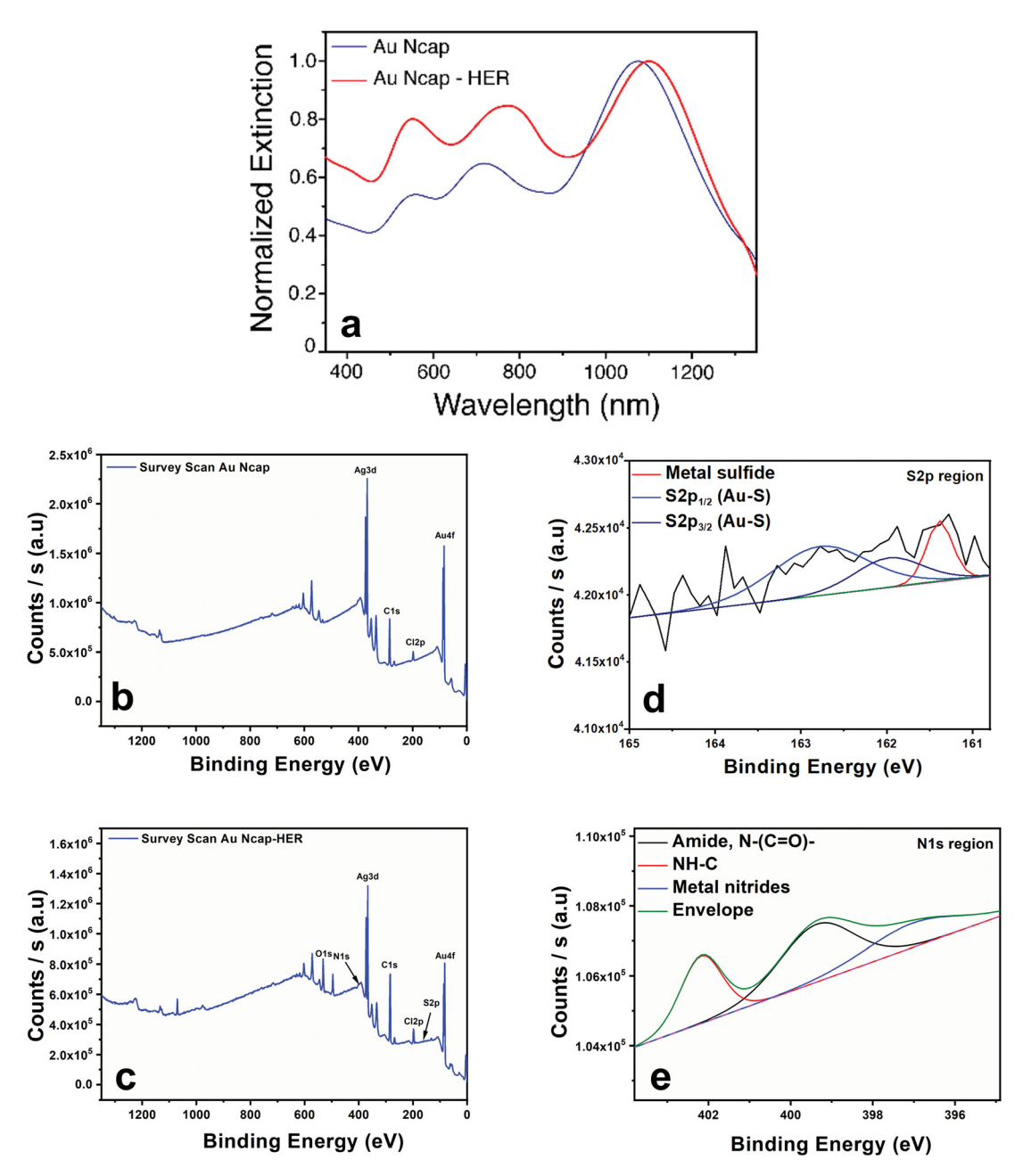


Fig. 2 (a) UV-Vis-NIR spectra of Au Ncap before and after Herceptin conjugation. XPS survey scan of (b) bare Au Ncap, and (c) Herceptin-functionalized Au Ncap. Deconvoluted XPS peaks of the (d) S 2p (e) N 1s regions for Herceptin-conjugated Au Ncap, respectively.

laser irradiation, a temperature increase ( $\Delta T$ ) of 27 °C was observed in the solution at a concentration of 50 μg mL<sup>-1</sup> and a power density of 3 W cm<sup>-2</sup>. Additionally, at a constant laser power of 0.5 W cm<sup>-2</sup>, a concentration-dependent (25 μg mL<sup>-1</sup> to 100 μg mL<sup>-1</sup>) temperature rise in the Au Ncap solution was noted (Fig. 3b). After 6 minutes of laser irradiation, the temperature  $(\Delta T)$  of the solution increased by approximately 11 °C at the highest concentration of Au Ncap tested (100 µg mL<sup>-1</sup>) demonstrating the excellent photothermal property of the prepared Au Ncap. The photothermal stability of the Au Ncaps was further evaluated by continuously irradiating the Au Ncap

colloidal aqueous solution at a power density of 0.5 W cm<sup>-2</sup> for 6 consecutive laser on/off cycles (Fig. 3c). No decline in the photothermal response of the Au Ncaps was observed during repeated laser on/off cycles, demonstrating the excellent photothermal stability of the Au Ncaps. Subsequently, the photothermal conversion efficiency  $(\eta)$  of the Au Ncaps was determined using eqn (1).20,32,35,36

$$\eta = \frac{hs(T_{\text{max}} - T_{\text{surr}}) - Q_{\text{Dis}}}{I(1 - 10^{-A_{1064}})} \tag{1}$$

**RSC Pharmaceutics** Paper

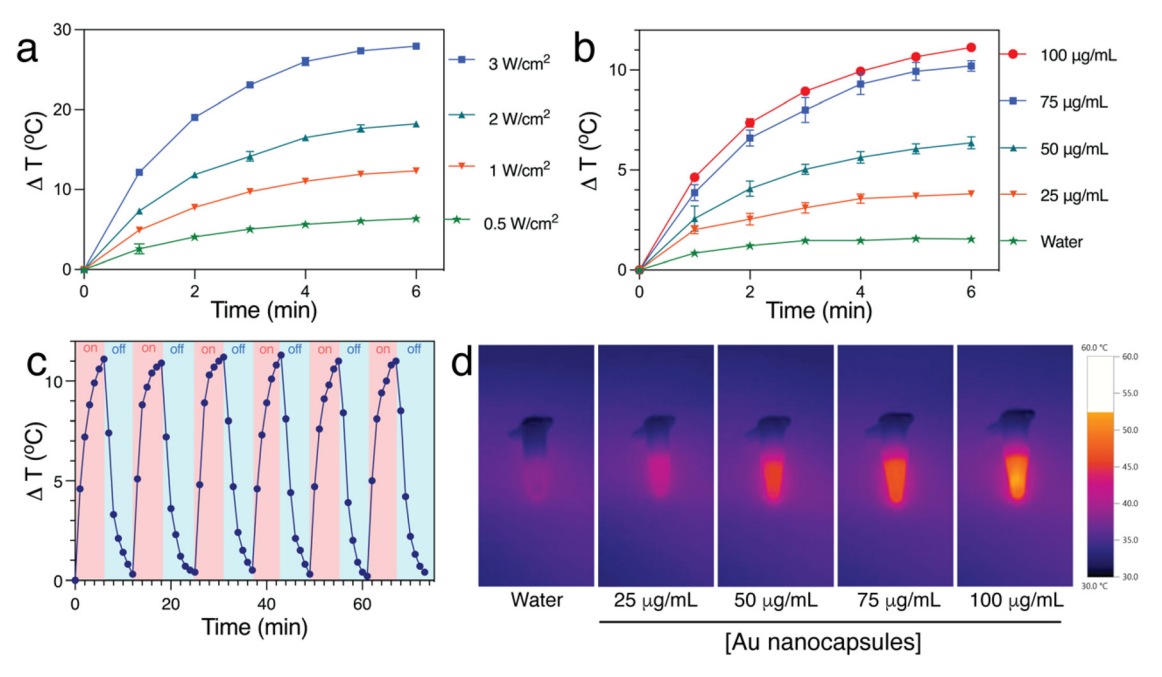


Fig. 3 Photothermal performance of Au Ncap. (a) Temperature profiles of Au Ncap at varying laser power densities (0.5, 1, 2, and 3 W cm<sup>-2</sup>) during 1064 nm laser irradiation at a concentration of 50  $\mu$ g mL $^{-1}$  for 6 minutes each. (b) Temperature profiles of different concentrations (10, 20, 50, and 100  $\mu g$  mL<sup>-1</sup>) subjected to 1064 nm laser irradiation at 0.5 W cm<sup>-2</sup> for 6 minutes each. (c) Photothermal stability cycle of aqueous gold nanocapsule solution over consecutive laser on/off cycles at a power density of 0.5 W cm<sup>-2</sup> using a concentration of 100 µg mL<sup>-1</sup>. (d) Thermal IR images of colloidal solution of Au Ncap at various concentrations after laser irradiation.

where, 'h' represents the heat transfer coefficient, 's' denotes the surface area of the container holding the Au Ncap solution during laser irradiation,  $T_{\text{max}}$  is the maximum temperature rise of the solution, and  $T_{\text{surr}}$  is the initial temperature of the solution. 'I' refers to the laser power output in mW,  $A_{1064}$  is the absorbance of the Au Ncap at the experimental concentration at 1064 nm, and  $Q_{\rm dis}$  indicates the power output of the solvent medium in the container, measured in mW. The 'hs' value was determined using a dimensionless parameter  $(\theta)$  as given below in eqn (2).

$$\theta = \frac{T - T_{\text{surr}}}{T_{\text{max}} - T_{\text{surr}}}.$$
 (2)

The sample time constant 't' was calculated using eqn (3)

$$t = -\tau_{\rm s} \ln(\theta). \tag{3}$$

A graph for eqn (3) was plotted and the slope was used to determine the  $\tau_s$  value of Au Ncap (Fig. S2†). The value of 'hs' was calculated from eqn (4).

$$hs = \frac{m_{\rm D}C_{\rm D}}{\tau_{\rm s}} \tag{4}$$

where,  $m_D$  = weight of the solution in g, CD = 4.187 J per g per °C is the heat capacity of the solution. A photothermal conversion efficiency ( $\eta$ ) of 38.6% was calculated using a 1064 nm laser, which was significantly higher than that of several previously reported gold nanostructures.<sup>37</sup> Additionally, the photothermal heating performance of the gold nanocapsules was confirmed by capturing thermal images of gold nanocapsules at different concentrations after laser irradiation at 3 W cm<sup>-2</sup> (Fig. 3d). We further compared the photothermal heating performances of bare gold nanocapsules, Au Ncap-PEG, and Herceptin-conjugated gold nanocapsules at a concentration of 50 μg ml<sup>-1</sup> with a laser power of 0.5 W cm<sup>-2</sup> (Fig. S3†). The results showed similar heating performances, with a slight decrease in the heating efficiency of the gold nanocapsules after Herceptin conjugation. This reduction in heating performance of the Au Ncap-Her is likely due to the presence of additional PEG polymer and Herceptin on the surface of the gold nanocapsules.

In vitro biocompatibility and targeted in vitro photothermal therapy using Herceptin conjugated Au Ncap. The in vitro biocompatibility of Au Ncap-HER with the HEK-293A cell line was assessed before proceeding with the in vitro PTT applications. HEK-293A cells were treated with various concentrations of Au Ncap-HER (ranging from 10 to 100  $\mu$ g mL<sup>-1</sup>) for 24 h. After the removal of the nanoparticle-containing media, the cells were washes with PBS. Cellular viability of the treated cells was then calculated using an XTT-based cell viability assay. No evidence of toxicity was observed, and cell viability remained well above 90%, even at the highest concentration measured (Fig. 4a), indicating the biocompatibility of Herceptin-conjugated Au

To evaluate the targeted in vitro PPTT action of the nanocapsules in breast cancer SK-BR-3 cells, the cellular uptake of Au Ncap with and without Herceptin conjugation was first

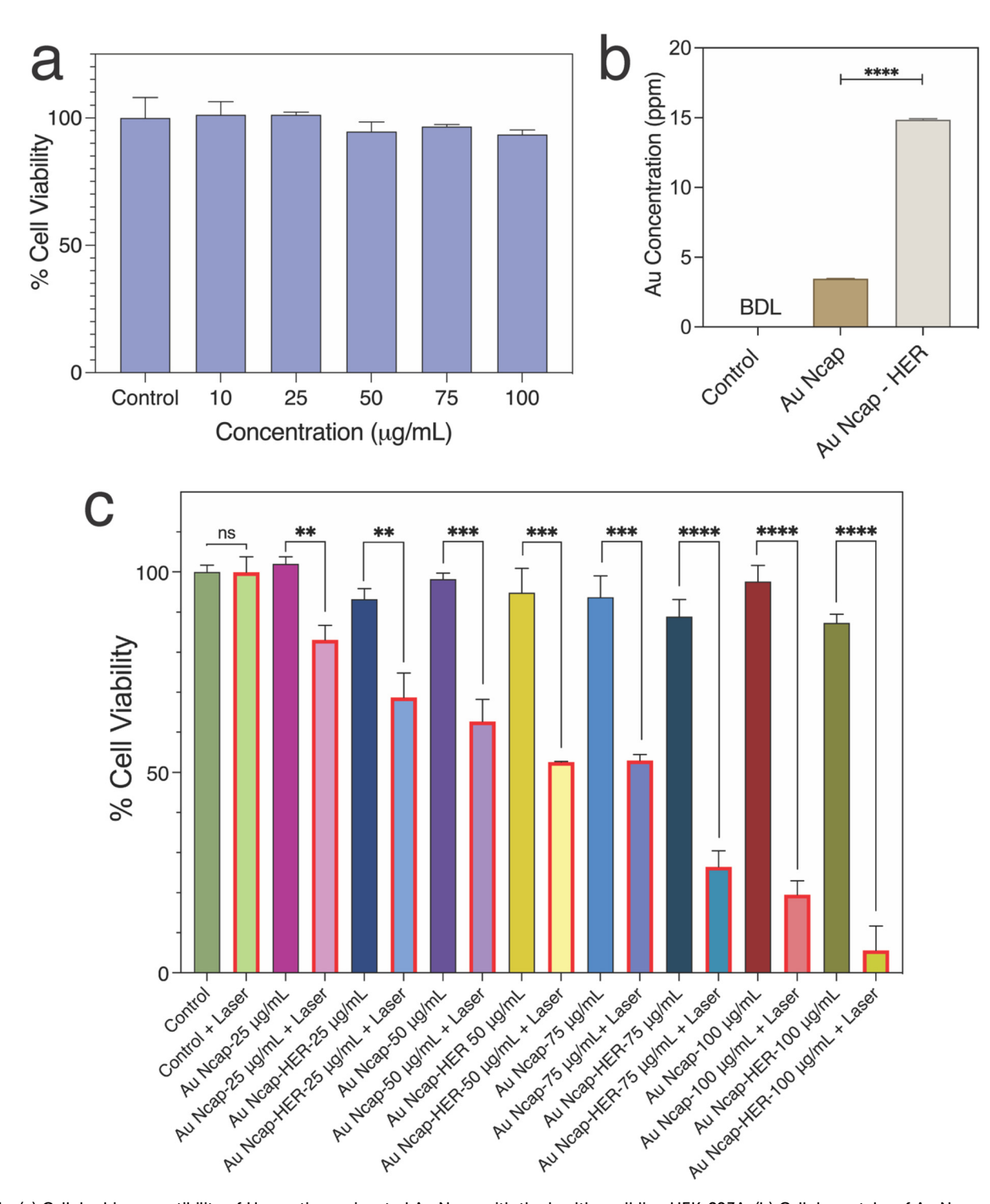


Fig. 4 (a) Cellular biocompatibility of Herceptin-conjugated Au Ncap with the healthy cell line HEK-293A. (b) Cellular uptake of Au Ncap with and without Herceptin conjugation, determined using ICP-MS to measure the amount of gold in SK-BR-3 cells (\*\*\*\* p < 0.0001). (c) Cell viability analysis for targeted and non-targeted photothermal therapy against SK-BR-3 cells using Au Ncap. Laser-treated samples were exposed to a laser power density of 0.5 W cm<sup>-2</sup> (\*\* p < 0.001, \*\*\* p < 0.001, \*\*\* p < 0.0001).

assessed using ICP-MS. The concentration of metal present in the SK-BR-3 cells after 6 hours of nanoparticle incubation was determined, as represented in Fig. 4b. The ICP-MS results indicated that after Herceptin conjugation, the uptake of Au Ncap increased threefold compared to the non-conjugated gold nanocapsules. This data demonstrates the targeted delivery of Au Ncap-HER to SK-BR-3 cells.

The *in vitro* photothermal potential of Au Ncap was then evaluated in SK-BR-3 cells. The photothermal effect on the cells was investigated using both HER conjugated and non-

conjugated Au Ncap at concentrations of 25, 50, 75, and 100 μg mL<sup>-1</sup>. The Au Ncap, without Herceptin, was rendered biocompatible by surface modification using m-PEG5000-SH. After 6 hours of Au Neap incubation, the media containing nanocapsules was removed and replaced with fresh cell culture media after rinsing with PBS. The cells were then subjected to

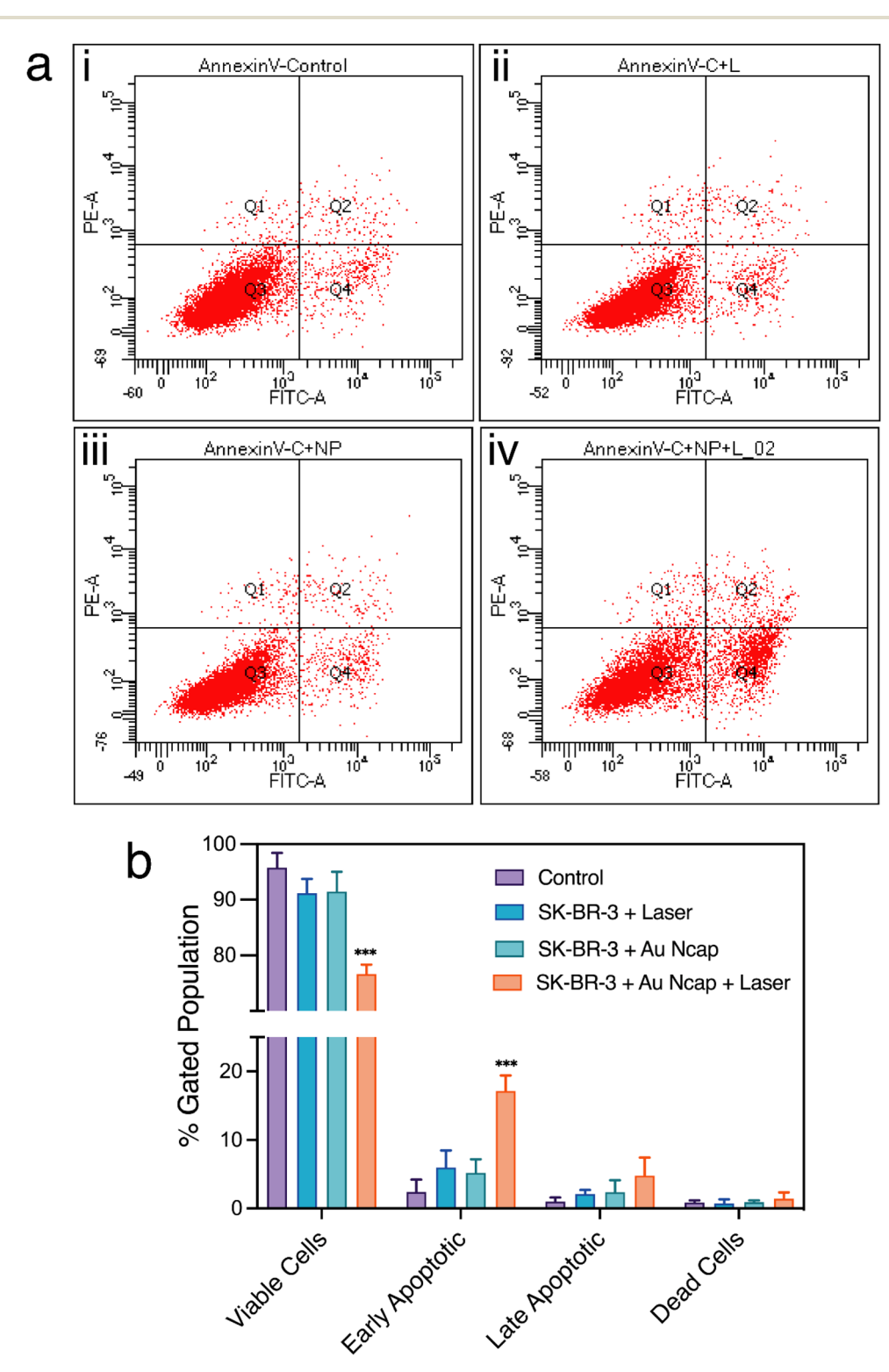


Fig. 5 (a) Flow cytometric scatter plots showing annexin V-FITC/PI staining in untreated SK-BR-3 cells, laser-treated SK-BR-3 cells, SK-BR-3 cells treated with Au-Ncap-HER, and SK-BR-3 cells incubated with Au Ncap-HER followed by laser irradiation. The cells were treated with 100 µg ml<sup>-1</sup> Herceptin-conjugated Au Ncap for 6 hours before being exposed to a 1064 nm laser at 0.5 W cm<sup>-2</sup> for 10 minutes. (b) The plot represents the fraction of cells in each phase of cell death relative to the gated population (\*\*\*p < 0.001).

a 1064 nm laser with a power density of 0.5 W cm<sup>-2</sup> for 10 minutes. Following laser irradiation, the SK-BR-3 cells were incubated at 37 °C in a 5% CO<sub>2</sub> environment. After 18 hours, the percentage of cell viability in laser-treated and control SK-BR-3 cells was assessed using an XTT-based cell viability assay. For Au Ncap without Herceptin, the percentage of cell viability was 83.1%, 62.7%, 53%, and 19.5% for concentrations of 25, 50, 75, and 100 µg mL<sup>-1</sup>, respectively. In contrast, for Herceptin-conjugated gold nanocapsules at the same concentrations, the percentage of cell viability was 68.7%, 52.6%, 26.5%, and 5.6% (Fig. 4c). The increase in cell death to nearly 96% after laser treatment at 100 μg mL<sup>-1</sup> of Au Ncap-HER demonstrated the nanoparticles' excellent PPTT potential, indicating their effective use in cancer therapy. A significant increase in cell death in the case of Au Ncap-HER compared to bare Au Ncap can be attributed to the high cellular uptake of Herceptin conjugated gold nanocapsules versus non-conjugated Au Ncap, resulting in a significant localised temperature rise within the cells, promoting hyperthermia. This finding suggests that the Herceptin conjugated Au Ncap have outstanding potential for targeted photothermal therapy.

### 3.3. Elucidation of the mechanism of Au Ncap based photothermal cell death

Subsequently, the mechanism of cell death was determined by flow cytometry using annexin-V-FITC and PI staining assays. The fraction of cells in the early and late apoptotic phases was assessed for control SK-BR-3 cells, SK-BR-3 cells treated with a 1064 nm laser, SK-BR-3 cells treated with Au Ncap-HER, and SK-BR-3 cells treated with both Au Ncap-HER and a 1064 nm laser (Fig. 5a). In control SK-BR-3 cells, the fraction of cells in the early and late apoptotic phases was 2.4% and 1.0%, respectively. In contrast, for Au Ncap-HER and laser-treated SK-BR-3 cells, the percentage of cells in the early and late apoptotic phases was 17.1% and 4.8%, respectively (Fig. 5b). A slight increase in the early and late apoptotic phases was also observed in cells treated with the NIR laser and Au Ncap-HER; however, this increase was non-significant compared to the

control cells. This data confirmed that the Au Ncap-HER mediated PPTT induces an apoptotic mode of cell death.

The morphology of the cells after PPTT using Au Ncap-HER was further visualized using SEM. In control SK-BR-3 cells, a smooth surface and overall well-stretched cellular morphology were observed (Fig. 6a). However, in treated SK-BR-3 cells, a loss of morphology was noted, with the cells appearing rounded and shrunken (Fig. 6b). Additionally, a very rough surface, along with the presence of membrane blebbing and apoptotic bodies, was observed.<sup>3,32</sup> This observation clearly validates that apoptosis was induced as the mode of cell death by gold nanocapsules during PPTT.

### 4. Conclusion

In conclusion, this study highlights the successful synthesis and functionalization of gold nanocapsules (Au Ncaps) for targeted plasmonic photothermal therapy applications, particularly in the NIR-II region using a 1064 nm laser. The Au Ncaps demonstrated remarkable photothermal stability and a high photothermal conversion efficiency of 38.6%, even at a low laser power density of 0.5 W cm<sup>-2</sup>, which is considered safe for human exposure. The prepared Au Ncaps were rendered biocompatibility by PEGylation, and their targeting ability was significantly improved by conjugating them with Herceptin, a therapeutic agent specific to Her2-overexpressing SK-BR-3 breast cancer cells. This conjugation led to a substantial increase in nanoparticle uptake by the SK-BR-3 cells, resulting in more effective and targeted PPTT.

The *in vitro* studies confirmed that the Herceptin-conjugated Au Ncaps exhibited superior photothermal performance compared to non-conjugated nanocapsules, effectively inducing apoptotic cell death with a marked reduction in cell viability. Flow cytometry and SEM analyses further validated that the Au Ncap-HER-mediated PPTT induces apoptosis as the primary mode of cell death. This work not only demonstrates the enhanced photothermal and therapeutic efficacy of the developed gold nanocapsules in the NIR-II region but also decodes the mechanism of cancer cell death, establishing Au

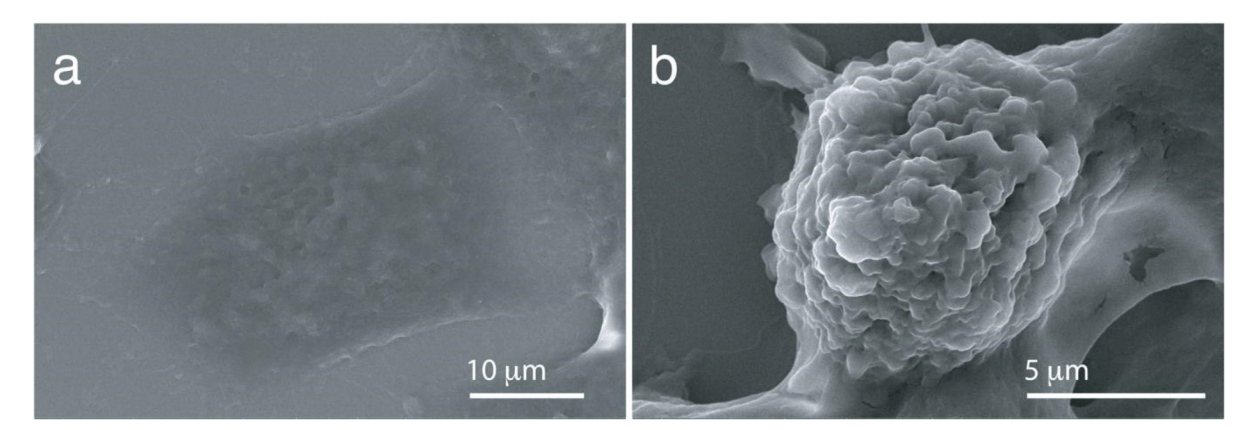


Fig. 6 SEM images of SK-BR-3 cells: (a) untreated and (b) laser-treated SK-BR-3 cells following incubation with Herceptin conjugated Au Ncap.

Ncap-HER as a promising candidate for targeted cancer therapy with potential clinical applications.

### Data availability

The datasets used and/or analyzed during the current study are available from the corresponding author on reasonable request. The data supporting this article have been included as part of ESI.†

### Conflicts of interest

The authors declare no conflict of interest.

### Acknowledgements

The work was supported by Department of Biotechnology (DBT), Government of India, under project number: BT/ PR14749/NNT/28/954/2015. A. J. acknowledges the research and infrastructure support provided by the BioX Centre and Advanced Materials Research Centre (AMRC) at the Indian Institute of Technology Mandi. The financial support from the Department of Biotechnology (DBT), Government of India, under project number BT/PR14749/NNT/28/954/2015, is gratefully acknowledged. P. S. and A. S. would like to thank the Ministry of Education (MoE) for providing doctoral fellowships. The authors extend their appreciation to Dr Vinay Jain and Agilent Technologies, Manesar, Gurugram, India, for conducting the ICP-MS analysis to assess the cellular uptake of gold nanocapsules. The ToC was prepared using Biorender. com and the authors gratefully acknowledge it. The authors also acknowledge Dr Shounak Roy for his help in some of the cell based experiments.

### References

- 1 N. G. Greeneltch, A. S. Davis, N. A. Valley, F. Casadio, G. C. Schatz, R. P. Van Duyne and N. C. Shah, J. Phys. Chem. A, 2012, 116, 11863-11869.
- 2 L. C. Kennedy, L. R. Bickford, N. A. Lewinski, A. J. Coughlin, Y. Hu, E. S. Day, J. L. West and R. A. Drezek, Small, 2011, 7, 169-183.
- 3 A. Sarkar, S. Roy, P. Sanpui and A. Jaiswal, ACS Appl. Bio Mater., 2019, 2, 4812-4825.
- 4 D. Cabuzu, A. Cirja, R. Puiu and A. Mihai Grumezescu, Curr. Top. Med. Chem., 2015, 15, 1605-1613.
- 5 H. S. Han and K. Y. Choi, *Biomedicines*, 2021, 9, 305.
- 6 N. Gandra, C. Portz and S. Singamaneni, Adv. Mater., 2014, 26, 424-429.
- 7 N. G. Khlebtsov and L. A. Dykman, J. Quant. Spectrosc. Radiat. Transfer, 2010, 111, 1-35.

- 8 A. B. Bucharskaya, N. G. Khlebtsov, B. N. Khlebtsov, G. N. Maslyakova, N. A. Navolokin, V. D. Genin, E. A. Genina and V. V. Tuchin, Materials, 2022, 15, 1606.
- 9 X. Huang, I. H. El-Sayed and M. A. El-Sayed, in Cancer Nanotechnol., Springer, 2010, pp. 343-357.
- 10 J. Chen, C. Glaus, R. Laforest, O. Zhang, M. Yang, M. Gidding, M. J. Welch and Y. Xia, Small, 2010, 6, 811-
- 11 H. Liu, D. Chen, L. Li, T. Liu, L. Tan, X. Wu and F. Tang, Angew. Chem., Int. Ed., 2011, 50, 891-895.
- 12 X. Huang, P. K. Jain, I. H. El-Sayed and M. A. El-Sayed, Lasers Med. Sci., 2008, 23, 217-228.
- 13 P. Singh, S. Roy, P. Sanpui, A. Banerjee and A. Jaiswal, in Nanotechnology in Modern Animal Biotechnology, Springer, 2019, pp. 29-65.
- 14 A. C. Doughty, A. R. Hoover, E. Layton, C. K. Murray, E. W. Howard and W. R. Chen, *Materials*, 2019, **12**, 779.
- 15 N. D. Burrows, A. M. Vartanian, N. S. Abadeer, E. M. Grzincic, L. M. Jacob, W. Lin, J. Li, J. M. Dennison, J. G. Hinman and C. J. Murphy, J. Phys. Chem. Lett., 2016, 7,632-641.
- 16 E. Carbo-Argibay, B. Rodriguez-Gonzalez, I. Pastoriza-Santos, J. Perez-Juste and L. M. Liz-Marzan, Nanoscale, 2010, 2, 2377-2383.
- 17 P. Singh, K. Kundu, S. Seçkin, K. Bhardwaj, T. A. König and A. Jaiswal, Chem. - Eur. J., 2023, 29, e202302100.
- 18 P. Singh, S. Roy and A. Jaiswal, J. Phys. Chem. C, 2017, 121, 22914-22925.
- 19 P. Singh, T. A. König and A. Jaiswal, ACS Appl. Mater. Interfaces, 2018, 10, 39380-39390.
- 20 P. Singh and A. Jaiswal, ChemistrySelect, 2022, 7, e202103877.
- 21 S. Li, Q. Deng, Y. Zhang, X. Li, G. Wen, X. Cui, Y. Wan, Y. Huang, J. Chen and Z. Liu, Adv. Mater., 2020, 32, 2001146.
- 22 X. Wu, Y. Suo, H. Shi, R. Liu, F. Wu, T. Wang, L. Ma, H. Liu and Z. Cheng, Nano-Micro Lett., 2020, 12, 1-13.
- 23 Y. Chen, B. Sun, X. Jiang, Z. Yuan, S. Chen, P. Sun, Q. Fan and W. Huang, J. Mater. Chem. B, 2021, 9, 1002-1008.
- 24 Z. Wei, M. Wu, S. Lan, J. Li, X. Zhang, D. Zhang, X. Liu and J. Liu, Chem. Commun., 2018, 54, 13599-13602.
- 25 K.-W. Hu, T.-M. Liu, K.-Y. Chung, K.-S. Huang, C.-T. Hsieh, C.-K. Sun and C.-S. Yeh, J. Am. Chem. Soc., 2009, 131, 14186-14187.
- 26 A. Jaiswal, L. Tian, S. Tadepalli, K. K. Liu, M. Fei, M. E. Farrell, P. M. Pellegrino and S. Singamaneni, Small, 2014, 10, 4287-4292.
- 27 F. Gao, G. He, H. Yin, J. Chen, Y. Liu, C. Lan, S. Zhang and B. Yang, Nanoscale, 2019, 11, 2374-2384.
- 28 Y. Lyu, J. Li and K. Pu, Small Methods, 2019, 3, 1900553.
- 29 A. L. Antaris, H. Chen, K. Cheng, Y. Sun, G. Hong, C. Qu, S. Diao, Z. Deng, X. Hu and B. Zhang, Nat. Mater., 2016, 15, 235.
- 30 Q. Zhang, Q. Guo, Q. Chen, X. Zhao, S. J. Pennycook and H. Chen, Adv. Sci., 2020, 7, 1902576.

Paper

31 M. Mohl, A. Kumar, A. L. M. Reddy, A. Kukovecz, Z. Konya, I. Kiricsi, R. Vajtai and P. M. Ajayan, *J. Phys. Chem. C*, 2010, 114, 389–393.

- 32 P. Singh, P. Haloi, K. Singh, S. Roy, A. Sarkar, R. Choudhary, C. Mohite, S. Chawla, V. B. Konkimalla and P. Sanpui, *ACS Appl. Mater. Interfaces*, 2023, **15**, 39081–39098.
- 33 N. Nakajima and Y. Ikada, *Bioconjugate Chem.*, 1995, 6, 123–130.
- 34 P. K. Jain, W. Qian and M. A. El-Sayed, *J. Am. Chem. Soc.*, 2006, **128**, 2426–2433.
- 35 O. A. Savchuk, J. Carvajal, J. Massons, M. Aguiló and F. Díaz, *Carbon*, 2016, **103**, 134–141.
- 36 X. Liu, B. Li, F. Fu, K. Xu, R. Zou, Q. Wang, B. Zhang, Z. Chen and J. Hu, *Dalton Trans.*, 2014, 43, 11709– 11715.
- 37 Q. Tian, F. Jiang, R. Zou, Q. Liu, Z. Chen, M. Zhu, S. Yang, J. Wang, J. Wang and J. Hu, *ACS Nano*, 2011, 5, 9761–9771.